



1 **The impact of spatiotemporal structure of rainfall on flood**
2 **frequency over a small urban watershed: an approach coupling**
3 **stochastic storm transposition and hydrologic modeling**

4 Zhengzheng Zhou¹, James A. Smith², Mary Lynn Baeck², Daniel B. Wright³, Brianne K. Smith⁴,
5 Shuguang Liu¹

6 ¹Department of Hydraulic Engineering, Tongji University, Shanghai, China.

7 ²Department of Civil and Environmental Engineering, Princeton University, USA.

8 ³Department of Civil and Environmental Engineering, University of Wisconsin-Madison, USA.

9 ⁴Department of Earth and Environmental Sciences, City University of New York-Brooklyn College, USA.

10 *Corresponding to:* Zhengzheng Zhou (zhouzz@tongji.edu.cn); Shuguang Liu (liusgliu@tongji.edu.cn)

11 **Abstract.** The role of rainfall space-time structure, as well as its complex interactions with land surface properties, in
12 flood response remains an open research issue. This study contributes to this understanding, specifically in small (<15 km²)
13 urban watersheds. Using a flood frequency analysis framework that combines stochastic storm transposition-based rainfall
14 scenarios with the physically-based distributed GSSHA model, we examine the role of rainfall spatial and temporal
15 variability in flood frequency across drainage scales in the highly-urbanized Dead Run watershed (14.3 km²) outside of
16 Baltimore, Maryland, USA. The results show the complexities of flood response within several subwatersheds for both
17 short (<50 years) and long (>100 years) rainfall return periods. The impact of impervious area on flood response decreases
18 with increasing rainfall return period. For extreme storms, the maximum discharge is closely linked to the spatial structure
19 of rainfall, especially storm core spatial coverage. The spatial heterogeneity of rainfall increases flood peak magnitudes by
20 50% on average at the watershed outlet and its subwatersheds for both small and large return periods. The results imply
21 that commonly-made assumption of spatially uniform rainfall in urban flood frequency modeling is problematic even for
22 relatively small basin scales.

23 **1. Introduction**

24 Rainfall spatiotemporal structure plays an important role in flood generation in urban watersheds (Ogden *et al.*, 1995;
25 Saghafian *et al.*, 1995; Smith *et al.*, 2005b; Emmanuel *et al.*, 2012; Nikolopoulos *et al.*, 2014). Spatial heterogeneities in
26 land use and land cover complicate the translation of rainfall spatiotemporal distribution into flood responses (Galster
27 *et al.*, 2006; Morin *et al.*, 2006; Ntelekos *et al.*, 2008; Ogden *et al.*, 2011), especially for small catchments (Faurès *et al.*, 1995;
28 Smith *et al.*, 2005a; Zhou *et al.*, 2017). Due to the varying nature of rainfall and complexities of urban characteristics, the
29 influence of rainfall spatial-temporal structure on flood frequency analysis in urban areas remains an open research issue.



30 Many studies have examined the interaction between rainfall variability and flood response. By necessity, early studies
31 tended to explore rainfall variability using rain gages, which were the main source of rainfall measurements until relatively
32 recently. The accuracy of flood simulations using spatially-detailed rainfall scenarios has been examined (Dawdy and
33 Bergmann, 1969; Schilling, 1991), along with the sensitivity of hydrologic response to rainfall gage network density
34 (Faurès *et al.*, 1995; Arnaud *et al.*, 2002; Younger *et al.*, 2009; Notaro *et al.*, 2013). Beven and Hornberger (1982) argued
35 that the spatial variability affects the response time more than the peak magnitude, whereas Wilson *et al.* (1979) found the
36 reverse. These studies were limited, however, by the general sparsity of rain gages, which may not adequately capture the
37 spatial distribution of rainfall. Following the advent of rainfall measurement using weather radar (Fulton *et al.*, 1998;
38 Krajewski and Smith, 2002), many studies have highlighted the use of high-resolution rainfall data in assessing rainfall
39 variability over various range of spatial and temporal scales (Berne *et al.*, 2004; Gebremichael and Krajewski, 2004;
40 Moreau *et al.*, 2009; Emmanuel *et al.*, 2012) and how their use could improve runoff estimation (Morin *et al.*, 2006; Smith
41 *et al.*, 2007; Schellart *et al.*, 2012; Wright *et al.*, 2014b; Bruni *et al.*, 2015; Rafieeinassab *et al.*, 2015; Gourley *et al.*, 2017).
42 There are conflicting findings on the relative importance of rainfall temporal and spatial characteristics. Ochoa-Rodriguez
43 *et al.* (2015) and Yang *et al.* (2016), for example, found that “coarsening” temporal resolution has a stronger impact than
44 coarsening spatial resolution, especially for small watersheds. Similar results were found in the study of Paschalis *et al.*
45 (2014) in a 477 km² catchment in Switzerland. Adams *et al.* (2012) found the space-time averaging effects of routing
46 through the catchment noticeably remove the impact of spatially variable rainfall at a 150-km² catchment scale. Bruni *et al.*
47 (2015), in contrast, found a higher sensitivity of modeled flow peaks to spatial resolution rather than the temporal
48 resolution. Peleg *et al.* (2017) showed an increasing contribution of the spatial variability of rainfall to the variability of
49 flow discharge with longer return periods. Cristiano *et al.* (2018); Cristiano *et al.* (2019) found the spatial aggregation of
50 rainfall data can have a strong effect on hydrological responses. Zhu *et al.* (2018) examined the influence of rainfall
51 variability on flood frequency analysis and addressed the impact of antecedent moisture in flood generation for basin scales
52 ranging from 16 km² up to 4,400 km². Using observational data, Zhou *et al.* (2017) showed that the impact of antecedent
53 moisture is low in a highly-urbanized catchment.

54 Previous studies have demonstrated the sensitivity of hydrological response to rainfall variability in both space and time
55 (Smith *et al.*, 2012; Ochoa-Rodriguez *et al.*, 2015; Rafieeinassab *et al.*, 2015). The relationship between rainfall and flood
56 are scale-dependent, varying with rainfall patterns, basin characteristics, and runoff generation processes. However, there
57 is still no clear answer on the relative importance of temporal and spatial features of rainfall on flood responses (Cristiano
58 *et al.*, 2017). Moreover, studies focusing on small (< 15 km²) urbanized basins are relatively few (Peleg *et al.*, 2017) and
59 the issues remain poorly understood.



60 Stochastic Storm Transposition (SST) was developed as a physically-based stochastic rainfall generator for rainfall
61 frequency analysis. Previous studies show that SST with relatively short-term records (10 or more years) of high-resolution
62 radar rainfall field can produce reasonable rainfall scenarios with spatial-temporal structure, which cannot be provided by
63 conventional methods (Wright *et al.*, 2013; Wright *et al.*, 2017; Zhou *et al.*, 2019). Coupled with hydrological models, the
64 SST-based framework can be used for multiscale rainfall frequency analysis and flood frequency analysis that accounts for
65 rainfall variability and surface characteristics (Wright *et al.*, 2014a; Perez *et al.*, 2019; Yu *et al.*, 2019; Wright *et al.*, 2020).
66 This study contributes to the interaction between rainfall variability and flood response over small-scale urbanized
67 watersheds (<15 km²) for a short-duration rainfall and quick hydrologic response setting. We build on the SST-based rainfall
68 study of Zhou *et al.* (2019) using the physically-based hydrological model implementation introduced by Smith *et al.* (2015)
69 in the Dead Run watershed outside of Baltimore, Maryland, USA by addressing the following questions: (1) How does
70 flood frequency in small urban watersheds vary with diverse space-time rainfall structure and rainfall magnitude? (2)
71 Among the space-time feature of rainfall, what are the dominant features that control flood peak distribution in small urban
72 watersheds?
73 Using a framework that combines high-resolution realistic SST- and radar-based rainfall scenarios with model-based flood
74 frequency analysis, we characterize the spatial and temporal features of rainfall events under different return periods and
75 examine their roles in determining flood frequency in small urban watersheds. The paper is organized as follows: in Section
76 2, we introduce the study region and describe the SST-based methodology, GSSHA model, and the metrics used to
77 characterize rainfall and flood response. In Section 3, we present model validation and analyses of flood frequency
78 distributions and rainfall-flood relationships. A summary and conclusions are presented in Section 4.

79 **2. Data and method**

80 **2.1 Study region and data**

81 The study focuses on the highly-urbanized 14.3 km² Dead Run (DR) watershed located west of Baltimore, Maryland, USA
82 (Fig. 1). DR is a tributary to the Gwynns Falls watershed, which is the principal study catchment of the Baltimore
83 Ecosystem Study (BES) (Pickett and Cadenasso, 2006). The basin has an impervious fraction of approximately 52.3%
84 (Table 1). The watershed has a dense network of six stream gauges with drainage areas ranging from 1.2 to 14.3 km² (Fig.
85 1; Table 1). The subwatersheds are developed after the implementation of the Maryland Stormwater Management Act of
86 1982 (Maryland, 1982) with many detention infrastructures such as small local ponds. The wealth of data for Dead Run
87 provides exceptional resources to examine rainfall and hydrologic response (Beighley and Moglen, 2002; Nelson *et al.*,
88 2006; Meierdiercks *et al.*, 2010; Smith *et al.*, 2015). For example, Meierdiercks *et al.* (2010) analyzed the impact of storm



89 drains and detention basins on a single storm event in DR, while Ogden *et al.* (2011) used the Gridded Surface Subsurface
90 Hydrologic Analysis (GSSHA) model to analyze the effects of storm drains, impervious area, and drainage density on
91 hydrologic response. Smith *et al.* (2015) created a DR model using GSSHA to examine the effects of storage and runoff
92 generation processes through analyses of a large number of storm events.

93
94 High resolution (15-min temporal resolution, 1-km² spatial resolution) radar rainfall fields for the 2000-2015 period were
95 derived from volume scan reflectivity fields from the Sterling, Virginia WSR-88D (Weather Surveillance Radar-1988
96 Doppler) radar. The Hydro-NEXRAD algorithms (Krajewski *et al.*, 2011; Seo *et al.*, 2011) which have been used in rainfall
97 and hydrological studies (Smith *et al.*, 2007; Lin *et al.*, 2010; Smith *et al.*, 2013; Wright *et al.*, 2014b; Zhou *et al.*, 2017)
98 are used to estimate rainfall from reflectivity fields. A network of 54 rain gauges in and around Baltimore City is used for
99 mean field bias correction of the radar rainfall. The reader is directed to Zhou *et al.* (2019) and references therein for further
100 details on the rainfall data and bias correction methods.

101 Instantaneous discharge data with a resolution of five minutes from the U.S. Geological Survey (USGS) were used for each
102 of the six gaged watersheds. Streamflow observations for the outlet station at Franklinton extend back to 1960, while the
103 DR1 – DR5 stations have records beginning in 2008.

104 **2.2 GSSHA Hydrological Model**

105 The distributed physics-based GSSHA model is used to simulate multi-scale flood response. GSSHA is a two-dimensional,
106 distributed-parameter raster-based (i.e. square computational cell-based) hydrologic modeling system. It uses explicit finite
107 difference and finite volume methods in two dimensions on a structured grid to simulate overland flow and in one dimension
108 to simulate channel flow (Downer and Ogden, 2004; 2006). Previous studies of the GSSHA model show that the model
109 with fine grid resolution can produce adequate simulations of flood response, especially when driven by high-resolution
110 radar rainfall fields (Sharif *et al.*, 2010; Sharif *et al.*, 2013; Wright *et al.*, 2014a; Cristiano *et al.*, 2019).

111 In this study, we use the Dead Run model created by Smith *et al.* (2015). A brief description of the model is provided here;
112 see Smith *et al.* (2015) for more details. The delineation of the watershed and channel network was based on a 30-m USGS
113 digital elevation model (Gesch *et al.*, 2002). Channel flow overland flow was set with different Manning's roughness
114 coefficients. Additional stream channels were added based on the Baltimore County hydrography Geographic Information
115 Systems (GIS) map. Stream cross sections were extracted from a 1-m resolution topography data set for Dead Run
116 developed from lidar. Storm sewers in DR-2 and DR-5 were added using the Baltimore County Stormwater Management
117 GIS map and digitized storm sewer maps. The semicircle's diameter was set to the pipe diameter. Detention basins were



118 represented within the channel with cross sections extracted from the 1-m lidar topographic data.
119 Several aspects of the model were modified from those used in Smith *et al.* (2015), primarily to improve computational
120 speed. Infiltration is calculated using Richards' equation (RE) in Smith *et al.* (2015), while this study uses the three-layer
121 Green-Ampt (GA) scheme. A uniform Manning's roughness coefficient of 0.01 is set for all the stream channels for model
122 simplification. Initial soil moisture is approximated to be one third of field capacity for each storm event.

123 2.3 SST procedure

124 The rainfall scenarios in this study are developed using RainyDay, an open-source SST software package (Wright *et al.*,
125 2017). The steps used are briefly summarized here; the reader is directed to Zhou *et al.* (2019) and references therein for
126 further details.

127 The first step is to identify a geospatial "transposition domain" that contains the watershed of interest. In this study, we use
128 a square 7,000 km² transposition domain centered on the DR watershed. (Zhou *et al.*, 2019) presented a detailed
129 examination of heterogeneity in extreme rainfall over the transposition domain using a variety of metrics, including storm
130 counts, mean storm depths and intensities, convective activity indicated by lightning observations, and analysis of spatial
131 and temporal rainfall structure.

132 The second step is to identify the largest m storms within the domain at the t -hr time scale. This collection of storms is
133 referred to as a storm catalog. The storms are selected with respect to the size, shape and orientation of the DR watershed.
134 We henceforth refer to these as "DR-shaped storms." The m DR-shaped storms are selected from an n -year rainfall record,
135 such that an average of $\lambda=m/n$ storms per record year are included in the storm catalog. In this study, we chose $m = 200$
136 storms over the 16-year radar record.

137 The third step is to randomly sample a subset of k storms from the storm catalog, where k refers to a stochastic number of
138 storms per year. The k is assumed to follow a Poisson-distributed number of storm occurrences with rate parameter $\lambda=m/n$
139 storms per year. All rainfall fields associated with a storm are transposed by an east-west distance Δx and a north-south
140 distance Δy , where Δx and Δy are drawn from distributions $D_x(x)$ and $D_y(y)$ which are bounded by the limits of the
141 transposition domain. Based on the spatial heterogeneity analysis of extreme rainfall in the domain, distributions $D_x(x)$ and
142 $D_y(y)$ can be set as uniform or non-uniform. In Zhou *et al.* (2019) and this study, since the assumption of regional
143 homogeneity cannot be relaxed, we used the non-uniform distribution. A two-dimensional probability density function
144 (PDF) of spatial storm occurrence (Wright *et al.*, 2017) and an intensity factor that rescales the rainfall magnitude (Zhou
145 *et al.*, 2019) are used as the basis for non-uniform spatial transposition (Fig. A1 in Appendix A). This step can be understood
146 as generating a "synthetic year" of extreme rainfall events over the domain based on resampling and transposing



147 observations. For each of the k transposed storms, compute the t -hr basin-average rainfall depth over the watershed. Among
148 the k rainfall depths, the maximum depth is retained as a synthetic t -hr annual rainfall maximum for the watershed, while
149 the transposed rainfall fields are saved for use as inputs to a GSSHA model simulation.

150 The fourth step simply repeats Step 3 many times to recreate multiple years of synthetic t -hour “annual” rainfall maxima
151 and associated transposed rainfall fields for the watershed. In this study, these steps are repeated 1,000 times and the ordered
152 “annual” maxima are used to generate rainfall return period estimates up to 500 years. 1,000 such realizations of 500-yr
153 series are generated, and the median value of 1,000 realizations are used to generate estimates for return periods up to 500
154 years.

155 **2.4 Characteristics of rainfall and hydrologic response**

156 **2.4.1 Spatio-temporal characteristics of rainfall**

157 Rainfall statistics were computed for each event, based on radar rainfall data at 15-min, 1-km² resolution, to characterize
158 the spatial and temporal variability of rainfall (following Smith *et al.* (2002); Smith *et al.* (2005b); see also Zoccatelli *et al.*
159 (2011) and Emmanuel *et al.* (2015)). Basin-average rainfall rate at time t during the storm is given by:

$$160 \quad M(t) = \int_0^T R(t, x) dx \quad (1)$$

161 where $R(t, x)$ is the rain rate at radar grid x at time t , and T is the time period of rainfall event. Peak basin-average rainfall
162 rate is denoted:

$$163 \quad M_{max} = \max\{M(t); t \in [0, T]\} \quad (2)$$

164 and storm total rainfall depth is:

$$165 \quad R_{sum} = \sum_0^T M(t) \quad (3)$$

166 To characterize the spatial properties of rainfall, several quantities are computed. Fractional coverage of storm core at t is
167 given by:

$$168 \quad Z(t) = \frac{1}{A} \int_A I_{(R(t,x))} dx \quad (4)$$

169 where $I_{(R(t,x))}$ is the indicator function and equals 1 when $R(t, x) > 25 \text{ mm/h}$ or 0 otherwise.

170 Rainfall location is given by:

$$171 \quad L(t) = \int_A \omega(t, x) d(x) dx \quad (5)$$



172 where $\omega(t, x) = \frac{R(t, x)}{\int_A R(t, x) dx}$, $d(x)$ is the linear distance from point x to the outlet. The rainfall-weighted flow distance is:

$$173 \quad \text{RWD}(t) = \int_A \omega(t, x) d_f(x) dx \quad (6)$$

174 where distance function $d_f(x)$ is the flow distance between point x and the outlet. It is calculated as the sum of the
175 overland flow distance from x to the nearest channel and the distance along the channel to the basin outlet. The flow distance
176 $d_f(x)$ is normalized by the maximum flow distance, ranging from 0 to 1. RWD with values close to 0 indicates that rainfall
177 is distributed near the basin outlet; with values close to 1 indicates rainfall concentrated at the far periphery of the basin.
178 For a uniformly distributed rainfall, the mean RWD is:

$$179 \quad \overline{\text{RWD}} = \int_A d_f(x) dx \quad (7)$$

180 The dispersion of RWD:

$$181 \quad S(t) = \frac{1}{\bar{s}} \int_A \omega(t, x) [d_f(x) - \bar{d}]^2 dx \quad (8)$$

182 where $\bar{s} = \int_A [d_f(x) - \bar{d}]^2 dx$, S is a spatial indicator with values < 1 indicates that rainfall is a unimodal distribution; S
183 with values > 1 indicates that rainfall is a multimodal distribution.

184 2.4.2 Spatiotemporal characteristics of hydrologic response

185 Flood peak (Q_{peak} , mm^3/s), total runoff (Q_{sum} , mm), and lag time (T_{lag} , min) are defined as:

$$186 \quad Q_{peak} = \max\{Q(t); t \in T_d\} \quad (9)$$

$$187 \quad Q_{sum} = \sum_0^{T_d} Q(t) \quad (10)$$

$$188 \quad T_{lag} = T_{Fpeak} - T_{Rpeak} \quad (11)$$

189 Respectively, where $Q(t)$ is the flow discharge at time t ; T_d is the duration of hydrological response, which is from the
190 start of rainfall event to the time when $f(t) < 0.05 \cdot Q_{peak}$.

191 3. Results and Discussion

192 3.1 Model validation

193 We validated the Dead Run GSSHA model through analyses of the 21 largest warm season (April-September) flood events
194 with peak discharges ranging from 70.3 to 253 m^3/s in the 2008-2012 period. The simulated discharge was compared to
195 USGS streamflow observations for all six gaging stations. We assessed the peak discharge and peak time to examine the



196 performance of the model. The GSSHA modeled and USGS gage measured hydrographs for three storm events are
197 compared in Fig. A2-A4 in Appendix A.

198 Peak discharge difference is calculated as the difference between the modeled peak and measured peak as a percentage of
199 the measured peak. Median peak discharge differences across all 21 events range from -35% to 57% (Fig. 2a). The largest
200 difference is in sub-basin DR-1. The reason is likely that DR-1 has a large area of land which was not represented fully on
201 county storm sewer maps (Smith *et al.*, 2015). The median peak discharge difference at the watershed outlet was -14%.
202 The peak time difference is calculated as the time difference between the simulated peak time and measured peak time (Fig.
203 2b). The median difference ranges from -15 to +10 minutes, which is within the temporal resolution of the data (15 minutes
204 for rainfall; 5 minutes for streamflow). The results show that the main tendency of flood response is captured by the model.
205 Overall, the validation shows that the physically-based, minimally-calibrated model can capture the main shape and timing
206 of the measured response in Dead Run. We therefore conclude that the model is suitable for the subsequent flood frequency
207 analysis. It should be noted that the errors in simulated response may be attributable to measurement errors tied to stage
208 discharge curves and to conversions of radar reflectivity to rainfall rate, as well as to the features that were simplified within
209 the model, such as initial soil moisture and some aspects of the storm drain network (Smith *et al.*, 2015).

210 **3.2 Flood frequency distribution**

211 Under the SST framework, 3-h rainfall scenarios for 10-yr, 50-yr, 100-yr and 200-yr return periods were generated (Fig.
212 A5 in Appendix A). We then simulated hydrographs using the GSSHA model and rainfall scenarios for Franklinton and
213 the five DR subwatershedss.

214 **3.2.1 Flow discharge estimates**

215 The distribution of maximum discharge at the Franklinton gage for rainfall return periods ranging
216 from 10 to 200 years is illustrated in Fig. 3a. To compare the distributions of rainfall and flood peaks,
217 the values are normalized to range from 0 to 1. The most striking feature is that the distributions of
218 total rainfall and flood peaks are highly variable across the four return periods. The kernel density
219 distribution of rainfall shows a peak at the position of 50th quantile for four return periods. The
220 distribution of flood peak is more complex. For the 100-yr rainfall return period, the kernel density
221 distribution of flood peaks shows a multimodal trend with two small peaks around the 25th and 75th
222 quantiles, which contrasts with the unimodal distribution of rainfall. For the 200-yr rainfall return
223 period, the interquartile range (IQR) is larger than other return periods. The relative standard deviation,



224 known as the coefficient of variation (CV), is used to present the dispersion of peak distribution. CV
225 is defined as the ratio of the standard deviation to the mean. Unlike the IQR results, CV decreases with
226 increasing return period. According to Zhou *et al.* (2019), the variability of basin-average total rainfall
227 increases with return period. The pronounced difference in the distributions of total rainfall and flood
228 peaks highlights a complex relationship between rainfall properties and flood response in this relatively
229 small urbanized watershed.

230 The flood response time is calculated as the difference between the time of maximum rainfall rate and
231 maximum discharge (Fi. 3b). Median values of response time are similar under all return periods,
232 ranging from 70 to 83 minutes, which, given the temporal resolution of rainfall is 15 minutes, can be
233 similar for all four return periods. It can be concluded that although the flood peak magnitude increases
234 with rainfall return period, the response time is consistent for various rainfall scenarios. This implies
235 in this small highly urbanized watershed the response time is more linked to the drainage system rather
236 than to rainfall characteristics.

237 Figure 4 demonstrates the simulated hydrographs for the four return periods. The upper and lower
238 spread (75th and 25th quantiles) of the hydrograph indicates the range of variability of simulated
239 hydrographs. For the 10-yr return period, the hydrograph is relatively smooth with smaller spread.
240 With increasing return period, the hydrograph is peakier with shorter duration of high magnitude
241 discharge. The hydrograph for the 50-yr return period shows a transitional shape between small (10-
242 yr) and large (100-yr and 200-yr) rainfall return periods. For the 100-yr return period, the upper spread
243 shows a tendency toward dual peaks, which cannot be revealed from conventional design flood
244 practices. For the 200-yr return period, the hydrograph is peakiest with a large upper spread.

245 3.2.2 Spatial distribution of flood magnitude

246 The distribution of flood peaks over the five subwatersheds exhibits contrasting variation with rainfall return periods
247 ranging from 10 to 200 years (Fig. 5). Generally, basin scale plays an important role in determining the distribution of flood
248 magnitudes. Under the 10-yr rainfall return period, DR1 and DR2, with basin scales of 1.3 and 2.0 km², have higher flood
249 peaks and interquartile ranges than other subwatersheds. DR5 (2.1 km²) has comparable flood magnitude with DR4 (6.3
250 km²) and Franklinton (14.3 km²), while has a larger interquartile range than the latter two. DR3 with a basin scale of 4.95
251 km², has comparable flood magnitudes with DR1 and DR2. Under the 200-yr rainfall return period, DR2 and DR3 has a
252 slightly larger flood magnitude than DR1. DR5 has the largest interquartile range than others, though its flood peaks are



253 smaller than other small watersheds.

254 Results show that sub-basin flood distributions vary significantly with rainfall return periods. DR1 with larger impervious
255 area and detention controlled area than DR2 (Table 1), has larger flood peaks under small rainfall return period. For large
256 return periods, DR2 has larger peak and interquartile range than DR1, implying that flood peaks are less impacted by
257 impervious area for extreme storms. DR5, with the smallest detention controlled area by detention infrastructure, has the
258 smallest flood peaks under small rainfall return period. Under large return period, however, it has the largest changes in
259 peak discharges with comparable flood peaks with subwatersheds larger than 6 km². DR3 and DR4, with basin scale of
260 4.95 and 6.29 km², have contrasting flood magnitude under small and large return periods. DR3 with larger impervious
261 area and detention controlled area has larger flood peaks than DR4. The difference is more significant for small rainfall
262 events with the median value of flood peak for DR3 more than double that of DR4. From these results, it can be concluded
263 that impervious area and detention controlled area play a significant role in determining the peak discharges, but the
264 impact reduces with increasing rainfall return period. The less detention controlled sub-basin has larger flood variability
265 under large return period. The detention infrastructure impacts flood peak and its variability.

266 We further examine the spatial distribution of flood magnitude over the Dead Run watershed under the 100-yr return period
267 of flood at Franklinton (Fig. 6). The dimensionless flood index is used to compare flood peak magnitudes over the
268 watershed (Lu *et al.*, 2017). The flood index is computed as the maximum flow discharge divided by the computed 10-yr
269 flood (Q_{10-y}) at the same location, which is set as the median value of 10-yr peak discharge at the watershed outlet for each
270 100-yr design storm simulation. At Franklinton, the flood index and its interquartile range are largest across the
271 watersheds, with the median value greater than 2.5. The flood index in the five sub-watersheds is relatively lower, within
272 a median value between 1.5 and 2. DR2, as a sub-watershed of DR3, has a larger median value than DR1 and DR3. The
273 flood indices at DR1 and DR3 have similar median values and interquartile ranges. Values in DR4 are higher than its sub-
274 watershed, DR5, with a median value of 2. The variability of flood magnitudes, indicated by the CV, is stable among the
275 watersheds, ranging from 0.30 to 0.39. The spatial distribution of flood magnitude points to the significant heterogeneity
276 of flood distributions over the 14.3-km² watershed. For storm events that produce the same peak discharge return period at
277 the watershed outlet, the subsequent upstream flood response can vary substantially in the Dead Run watershed.

278 **3.3 Rainfall-Flood Relationships**

279 **3.3.1 Rainfall structure and flood response**

280 We investigate the relationship between the spatial and temporal characteristics of rainfall and flood response for small and
281 large rainfall return periods based on Spearman's rank correlation (Fig. A6 in Appendix A). The peak rainfall rate (M_{max}),



282 total rainfall (R_{sum}), fractional coverage (Z), rainfall location (L), rainfall-weighted flow distance (RWD) and the dispersion
283 of RWD (S) are used to characterize rainfall spacetime structure. For the 10-yr return period, the flood peak is somewhat
284 correlated with total rainfall, peak rainfall rate and storm core coverage with correlation coefficient of 0.16. For the 200-yr
285 return period, in contrast, there is no significant correlation between these features with correlation coefficients of -0.09,
286 0.07 and -0.02, respectively, implying a complex and nonlinear relationship between extreme storms and floods in the
287 watershed.

288 We used random forest regression models to examine the importance of rainfall characteristics to the flood response.
289 Rainfall spacetime structure characteristics are used as RF model features. The flood peak is set as the model target. The
290 main parameters of RF model are tuned by a grid search approach (Probst *et al.*, 2019). The prediction performance is
291 assessed using Mean Absolute Error (MAE), Root Mean Square Error ($RMSE$), and explained variance regression score (E
292 score) (Achen, 2017). Smaller values of MAE and $RMSE$ indicate better model performance. E score ranges from 0 to 1 and
293 a larger value indicates a better model (The training process of RF model is shown in Fig. A7 in Appendix A). The difference
294 in feature importance is compared between the 10-yr and 200-yr return periods (Fig. 7). For the 10-yr return period, peak
295 rainfall rate (M_{max}) and total rainfall (R_{sum}) are the most two important features. For the 200-yr return period, however, the
296 dispersion of RWD (S) and fractional coverage of storm core (Z) are more important than peak rainfall rate and total rainfall.
297 The rainfall location (L) has the smallest importance for both return periods. The results demonstrate the different
298 relationships between rainfall structure and flood response under small and extreme rainfall events. For extreme storms,
299 the maximum discharge is more closely linked to the spatial structure of rainfall, which is consistent with the results in
300 (Peleg *et al.*, 2017; Zhu *et al.*, 2018).

301 The temporal shapes of hydrographs and hyetographs are compared by using the coefficient of skewness (Fig. 8). The
302 skewness is used to assess the shape of rainfall process and discharge process. A negative value of skew indicates a left tail
303 of the distribution, and positive indicates a right tail. For the 10-yr return period, the rainfall skewness ranges from -0.1 to
304 3.5, demonstrating the mixed shapes of temporal distribution. Similar features are found for discharge shapes. For the 200-
305 yr return periods, the skewness of discharge is mostly positive while the skewness of rainfall events still varies from -1 to
306 2.5. The general conclusion of these analyses is that regardless of the temporal distribution of rainfall, the flood response
307 is relatively rapid, highlighting the role of the urban drainage system for the hydrographic response. The relationship
308 between the variability of discharge and rainfall is not significant for the four return periods, which implies that in a highly-
309 urbanized watershed, the drainage system smooths rainfall variability somewhat.



310 **3.3.2 Rainfall return period vs. flood return period**

311 In conventional design storm/flood practices, the return period of rainfall and peak discharge is often assume to be
312 equivalent (Rahman *et al.*, 2002). Under the SST framework, we can examine this assumption (Wright *et al.*, 2014a). For
313 each SST realization containing 100 rainfall scenarios with return period from 5 years up to 100 years, the peak discharge
314 can be simulated and ordered. Flood frequency for return periods from 5 years up to 100 years are then estimated from the
315 ordered peaks. We run 30 SST realizations in total. The Spearman's rank correlation of the two return periods is 0.5 (Fig.
316 9). The results quantitatively confirm that the assumption of a 1:1 return period equivalency between design storm and
317 design flood cannot hold, even in a small highly-urbanized watershed where drainage network and rainfall structure play
318 an important role in flood response.

319 **3.3.3 Impact of rainfall spatial heterogeneity on flood responses**

320 We also compared the simulated flood response resulting when rainfall is uniform over the watershed, rather than spatially
321 distributed as in previous analyses (Fig. 4 and Table 2). Generally, the flood peaks generated from uniform rainfall have
322 lower peaks than for non-uniform rainfall. The difference increases with return period. Under the 10-yr return period, the
323 shapes of the two hydrographs have similar upper and lower bounds (75% and 25% quantiles). The median flood peak
324 using non-uniform scenarios is 22% higher than the uniform scenarios. Under the 200-yr return period, the hydrograph
325 resulting from non-uniform rainfall is much peakier than the uniform SST scenarios with higher upper and lower bounds.
326 The lower bound of hydrograph by non-uniform SST scenarios is close to the median hydrograph of uniform SST scenarios.
327 The impact of rainfall spatial heterogeneity among the five subwatersheds is different. DR1, with a basin scale of 1.32 km²
328 and located in the north-west boundary of the watershed, was the least-impacted by rainfall spatial distribution for all return
329 periods. In DR2, on the other hand, which is similar in drainage area to DR1, the flood peak increased by 46% for the 200-
330 yr return period. For DR3 and DR4, the spatial heterogeneity of rainfall contributes more to the flood peaks in DR4 than
331 in DR3. The most striking difference in flood peaks is in DR5 for the 50-yr return period. The difference in flood magnitude
332 is 75%. As mentioned above, DR5 is the sub-basin with the least detention controlled area. This finding is likely tied to
333 the complex relationship between space-time rainfall structure and the drainage network. We can thus conclude that the
334 spatial heterogeneity of rainfall can increase flood peaks dramatically under both small and large return periods. The impact
335 increases with return period. This result shows that the assumption of spatially uniform rainfall will underestimate flood
336 frequency.



337 **4. Summary and conclusions**

338 This paper addresses the problem of the impacts of short-duration rainfall variability on hydrologic response in small
339 urbanized watershed. By coupling a high-resolution radar rainfall dataset and stochastic storm transposition (SST) with the
340 GSSHA distributed physics-based model (see also (Wright *et al.*, 2014a; Zhu *et al.*, 2018), the relationships between rainfall
341 spatiotemporal structure and urban flood response is examined. The main findings are as follows:

342 1. The flood frequency distributions for subwatersheds within the highly-urbanized 14.3 km² Dead Run watershed
343 demonstrates the complexities of flood response for both short and long rainfall return periods. Especially for 3-h extreme
344 storms, the distribution of flood peaks shows large variability. The variability of flood magnitude shows a pronounced role
345 of rainfall space-time structure in flood production. This calls into question the commonly-made design storm assumption
346 of spatially uniform rainfall. The response time is less affected by rainfall structure and appears to be more closely
347 associated with the basin scale and drainage network features.

348 2. The spatial heterogeneity of flood frequency over the 14.3-km² watershed is striking for the 100-yr return period. The
349 intercomparison between subwatersheds show that the impact of impervious area decreases with increasing return periods.
350 The subbasin with the least detention infrastructure shows the largest flood variability for long return periods. For the 100-
351 yr return period, the flood index of five subwatersheds are different from that of their downstream outlet. It shows that
352 storm events that produce the same peak discharge return period at the basin outlet can be the result of very different
353 upstream flood responses.

354 3. The relationship between the spacetime structure of rainfall and flood response is complex. The random forest-based
355 feature importance analysis shows very different relationships between rainfall structure and flood response for frequent
356 vs. extreme rainfall events. For smaller and more frequent rainfall events, flood peaks are more closely linked to the
357 temporal features of rainfall (total rainfall and peak rainfall rate). For extreme storms, the maximum discharge is closely
358 linked to the spatial structure of rainfall (storm core coverage). This finding is broadly consistent with (Peleg *et al.*, 2017)
359 and (Zhu *et al.*, 2018), despite the very different drainage scales considered in those studies. There is no significant
360 correlation between rainfall peak, total rainfall and flood peaks, implying an important role of surface properties in
361 urbanized watersheds. Similar to (Wright *et al.*, 2014a), this comparison calls into question the conventional design storm
362 assumption of a 1:1 equivalency between rainfall and flood peak return periods.

363 4. The spatial heterogeneity of rainfall is a key driver of flood response across scales. Relative to spatially uniform rainfall,
364 spatially distributed rainfall can increase flood peaks by 50% on average at the watershed outlet and its subwatersheds for
365 both small and large return periods. This finding is broadly consistent with prior results at much larger scales in an



366 agricultural setting ((Zhu *et al.*, 2018)) and suggests both spatial and temporal rainfall distributions need to be considered
367 in flood frequency analyses, even in relatively small urban watersheds. This study also implies that the drainage network
368 substantially alters the impact of rainfall characteristics on the runoff.

369 Coupling the GSSHA model and SST-based rainfall frequency analysis, this study provides an effective approach for
370 regional flood frequency analysis for urban watersheds. It can be used to explore the dominant control on the upper tail of
371 urban flood peaks, without many of the limiting assumptions associated with design storm methods. The study area could
372 be extended in future work with larger basin scales and by manipulating the spatial heterogeneity of basin characteristics
373 within GSSHA or other similar modeling systems.

374 **Acknowledgments**

375 This study was supported by the National Science Foundation of China (Grant 51909191).

376 **Data availability**

377 Radar data are archived at Princeton University and can be downloaded from the url
378 <http://arks.princeton.edu/ark:/88435/dsp01q524jr55d>.
379

380 **Author contributions.**

381 Main contributions from each co-authors are as follows. Zhengzheng Zhou contributed to computation and organization of
382 the paper. James A. Smith contributed to the supervision and writing. Mary Lynn Beack is responsible for generating the
383 radar rainfall data. Brianne K. Smith contributed to the construction of the initial hydrological model. Daniel B. Wright
384 contributed to the writing of the paper. Shuguang Liu contributed to the supervision and writing.
385

386 **Reference**

- 387 Achen, C. H. (2017), What Does “Explained Variance“ Explain?: Reply, *Political Analysis*, 2, 173-184.
388 doi:10.1093/pan/2.1.173
- 389 Adams, R., A. W. Western, and A. W. Seed (2012), An analysis of the impact of spatial variability in rainfall on runoff and
390 sediment predictions from a distributed model, *Hydrological Processes*, 26(21), 3263-3280. doi:10.1002/hyp.8435
- 391 Arnaud, P., C. Bouvier, L. Cisneros, and R. Dominguez (2002), Influence of rainfall spatial variability on flood prediction,
392 *Journal of Hydrology*, 260(1), 216-230. doi:10.1016/S0022-1694(01)00611-4



- 393 Beighley, R. E., and G. E. Moglen (2002), Trend Assessment in Rainfall-Runoff Behavior in Urbanizing Watersheds,
394 *Journal of Hydrologic Engineering*, 7(1), 27-34. doi:10.1061/(ASCE)1084-0699(2002)7:1(27)
- 395 Berne, A., G. Delrieu, J.-D. Creutin, and C. Obled (2004), Temporal and spatial resolution of rainfall measurements
396 required for urban hydrology, *Journal of Hydrology*, 299(3), 166-179. doi:10.1016/j.jhydrol.2004.08.002
- 397 Beven, K. J., and G. M. Hornberger (1982), Assessing the effect of spatial pattern of precipitation in modeling stream flow
398 hydrographs, *JAWRA Journal of the American Water Resources Association*, 18(5), 823-829. doi:10.1111/j.1752-
399 1688.1982.tb00078.x
- 400 Bruni, G., R. Reinoso, d. G. Van, N. C., F. H. L. R. Clemens, and J. A. E. Ten Veldhuis (2015), On the sensitivity of urban
401 hydrodynamic modelling to rainfall spatial and temporal resolution, *Hydrology and Earth System Sciences*, 19(2), 691-709.
402 doi:10.5194/hess-19-691-2015, 2015
- 403 Cristiano, E., M. C. ten Veldhuis, and N. van de Giesen (2017), Spatial and temporal variability of rainfall and their effects
404 on hydrological response in urban areas – a review, *Hydrology and Earth System Sciences*, 21(7), 3859-3878.
405 doi:10.5194/hess-21-3859-2017
- 406 Cristiano, E., M. C. ten Veldhuis, S. Gaitan, S. Ochoa Rodriguez, and N. van de Giesen (2018), Critical scales to explain
407 urban hydrological response: an application in Cranbrook, London, *Hydrol. Earth Syst. Sci.*, 22(4), 2425-2447.
408 doi:10.5194/hess-22-2425-2018
- 409 Cristiano, E., M.-c. ten Veldhuis, D. B. Wright, J. A. Smith, and N. van de Giesen (2019), The Influence of Rainfall and
410 Catchment Critical Scales on Urban Hydrological Response Sensitivity, *Water Resources Research*, 55(4), 3375-3390.
411 doi:10.1029/2018WR024143
- 412 Dawdy, D. R., and J. M. Bergmann (1969), Effect of rainfall variability on streamflow simulation, *Water Resources*
413 *Research*, 5(5), 958-966. doi:10.1029/WR005i005p00958
- 414 Downer, C. W., and F. L. Ogden (2004), GSSHA: Model to simulate diverse stream flow producing processes, *Journal of*
415 *Hydrologic Engineering*, 9(3), 161-174. doi:10.1061/(ASCE)1084-0699(2004)9:3(161)
- 416 Downer, C. W., and F. L. Ogden (2006), Gridded Surface Subsurface Hydrologic Analysis (GSSHA) User's Manual;
417 Version 1.43 for Watershed Modeling System 6.1.
- 418 Emmanuel, I., H. Andrieu, E. Leblois, and B. Flahaut (2012), Temporal and spatial variability of rainfall at the urban
419 hydrological scale, *Journal of Hydrology*, 430-431, 162-172. doi:10.1016/j.jhydrol.2012.02.013
- 420 Emmanuel, I., H. Andrieu, E. Leblois, N. Janey, and O. Payrastré (2015), Influence of rainfall spatial variability on rainfall-
421 runoff modelling: Benefit of a simulation approach?, *Journal of Hydrology*, 531, 337-348.
422 doi:10.1016/j.jhydrol.2015.04.058



- 423 Faurès, J.-M., D. C. Goodrich, D. A. Woolhiser, and S. Sorooshian (1995), Impact of small-scale spatial rainfall variability
424 on runoff modeling, *Journal of Hydrology*, 173(1), 309-326. doi:10.1016/0022-1694(95)02704-S
- 425 Fulton, R. A., J. P. Breidenbach, D.-J. Seo, D. A. Miller, and T. O'Bannon (1998), The WSR-88D rainfall algorithm,
426 *Weather and Forecasting*, 13(2), 377-395. doi:10.1175/1520-0434(1998)013<0377:TWRA>2.0.CO;2
- 427 Galster, J. C., F. J. Pazzaglia, B. R. Hargreaves, D. P. Morris, S. C. Peters, and R. N. Weisman (2006), Effects of urbanization
428 on watershed hydrology: The scaling of discharge with drainage area, *Geology*, 34(9), 713-716. doi:10.1130/g22633.1
- 429 Gebremichael, M., and W. F. Krajewski (2004), Assessment of the statistical characterization of small-scale rainfall
430 variability from radar: Analysis of TRMM ground validation datasets, *Journal of Applied Meteorology*, 43(8), 1180-1199.
431 doi:10.1175/1520-0450(2004)043<1180:AOTSCO>2.0.CO;2
- 432 Gesch, D. B., M. J. Oimoen, S. K. Greenlee, C. A. Nelson, M. J. Steuck, and D. J. Tyler (2002), The national elevation data
433 set, *Photogrammetric Engineering and Remote Sensing*, 68(1), 5-11.
- 434 Gourley, J. J., et al. (2017), The FLASH Project: Improving the Tools for Flash Flood Monitoring and Prediction across
435 the United States, *Bulletin of the American Meteorological Society*, 98(2), 361-372. doi:10.1175/bams-d-15-00247.1
- 436 Krajewski, W., and J. Smith (2002), Radar hydrology: rainfall estimation, *Advances in water resources*, 25(8-12), 1387-
437 1394. doi:10.1016/S0309-1708(02)00062-3
- 438 Krajewski, W. F., A. Kruger, J. A. Smith, R. Lawrence, C. Gunyon, R. Goska, B.-C. Seo, P. Domaszczynski, M. L. Baeck,
439 and M. K. Ramamurthy (2011), Towards better utilization of NEXRAD data in hydrology: an overview of Hydro-
440 NEXRAD, *Journal of hydroinformatics*, 13(2), 255-266. doi:10.2166/hydro.2010.056
- 441 Lin, N., J. A. Smith, G. Villarini, T. P. Marchok, and M. L. Baeck (2010), Modeling extreme rainfall, winds, and surge from
442 Hurricane Isabel (2003), *Weather and forecasting*, 25(5), 1342-1361. doi:10.1175/2010WAF2222349.1
- 443 Lu, P., J. A. Smith, and N. Lin (2017), Spatial Characterization of Flood Magnitudes over the Drainage Network of the
444 Delaware River Basin, *Journal of Hydrometeorology*, 18(4), 957-976. doi:10.1175/jhm-d-16-0071.1
- 445 State of Maryland. (1982), Department of the Environment : Water management, stormwater management.
- 446 Meierdiercks, K. L., J. A. Smith, M. L. Baeck, and A. J. Miller (2010), Analyses of urban drainage network structure and
447 its impact on hydrologic response, *JAWRA Journal of the American Water Resources Association*, 46(5), 932-943.
- 448 Moreau, E., J. Testud, and E. Le Bouar (2009), Rainfall spatial variability observed by X-band weather radar and its
449 implication for the accuracy of rainfall estimates, *Advances in Water Resources*, 32(7), 1011-1019.
450 doi:10.1016/j.advwatres.2008.11.007
- 451 Morin, E., D. C. Goodrich, R. A. Maddox, X. Gao, H. V. Gupta, and S. Sorooshian (2006), Spatial patterns in thunderstorm
452 rainfall events and their coupling with watershed hydrological response, *Advances in Water Resources*, 29(6), 843-860.



- 453 doi:10.1016/j.advwatres.2005.07.014
- 454 Nelson, P. A., J. A. Smith, and A. J. Miller (2006), Evolution of channel morphology and hydrologic response in an
455 urbanizing drainage basin, *Earth Surface Processes and Landforms*, 31(9), 1063-1079. doi:10.1002/esp.1308
- 456 Nikolopoulos, E. I., M. Borga, D. Zoccatelli, and E. N. Anagnostou (2014), Catchment-scale storm velocity: Quantification,
457 scale dependence and effect on flood response, *Hydrological Sciences Journal*, 59(7), 1363-1376.
458 doi:10.1080/02626667.2014.923889
- 459 Notaro, V., C. M. Fontanazza, G. Freni, and V. Puleo (2013), Impact of rainfall data resolution in time and space on the
460 urban flooding evaluation, *Water Science and Technology*, 68(9), 1984-1993. doi:10.2166/wst.2013.435
- 461 Ntelekos, A. A., J. A. Smith, M. L. Baeck, W. F. Krajewski, A. J. Miller, and R. Goska (2008), Extreme hydrometeorological
462 events and the urban environment: Dissecting the 7 July 2004 thunderstorm over the Baltimore MD Metropolitan Region,
463 *Water Resources Research*, 44(8), 1-19. doi:10.1029/2007WR006346
- 464 Ochoa-Rodriguez, S., L.-P. Wang, A. Gires, R. D. Pina, R. Reinoso-Rondinel, G. Bruni, A. Ichiba, S. Gaitan, E. Cristiano,
465 and J. van Assel (2015), Impact of spatial and temporal resolution of rainfall inputs on urban hydrodynamic modelling
466 outputs: A multi-catchment investigation, *Journal of Hydrology*, 531(2), 389-407. doi:10.1016/j.jhydrol.2015.05.035
- 467 Ogden, F. L., J. R. Richardson, and P. Y. Julien (1995), Similarity in catchment response: 2. Moving rainstorms, *Water*
468 *Resources Research*, 31(6), 1543-1547. doi:10.1029/95WR00519
- 469 Ogden, F. L., N. Raj Pradhan, C. W. Downer, and J. A. Zahner (2011), Relative importance of impervious area, drainage
470 density, width function, and subsurface storm drainage on flood runoff from an urbanized catchment, *Water Resources*
471 *Research*, 47(12). doi:10.1029/2011wr010550
- 472 Paschalis, A., S. Fatichi, P. Molnar, S. Rimkus, and P. Burlando (2014), On the effects of small scale space-time variability
473 of rainfall on basin flood response, *Journal of Hydrology*, 514, 313-327. doi:10.1016/j.jhydrol.2014.04.014
- 474 Peleg, N., F. Blumensaat, P. Molnar, S. Fatichi, and P. Burlando (2017), Partitioning the impacts of spatial and
475 climatological rainfall variability in urban drainage modeling, *Hydrology and Earth System Sciences*, 21(3), 1559.
476 doi:10.5194/hess-21-1559-2017
- 477 Perez, G., R. Mantilla, W. F. Krajewski, and D. B. Wright (2019), Using Physically Based Synthetic Peak Flows to Assess
478 Local and Regional Flood Frequency Analysis Methods, *Water Resources Research*, 55(11), 8384-8403.
479 doi:10.1029/2019WR024827
- 480 Pickett, S. T. A., and M. L. Cadenasso (2006), Advancing urban ecological studies: Frameworks, concepts, and results from
481 the Baltimore Ecosystem Study, *Austral Ecology*, 31(2), 114-125. doi:10.1111/j.1442-9993.2006.01586.x
- 482 Probst, P., M. N. Wright, and A. L. Boulesteix (2019), Hyperparameters and tuning strategies for random forest, *Wiley*



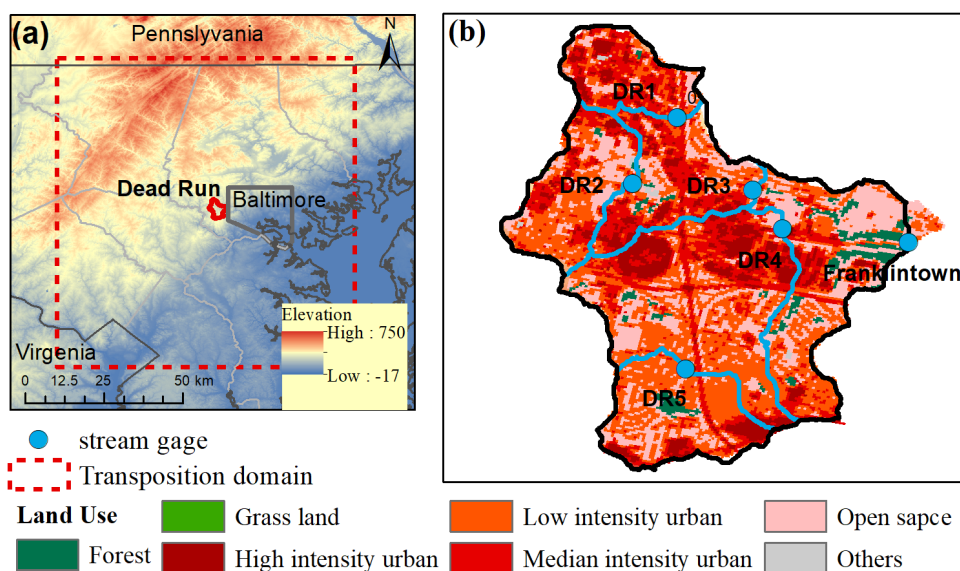
- 483 *Interdisciplinary Reviews: Data Mining and Knowledge Discovery*, 9(3), e1301. doi:10.1002/widm.1301
- 484 Rafieeinassab, A., A. Norouzi, S. Kim, H. Habibi, B. Nazari, D.-J. Seo, H. Lee, B. Cosgrove, and Z. Cui (2015), Toward
485 high-resolution flash flood prediction in large urban areas – Analysis of sensitivity to spatiotemporal resolution of rainfall
486 input and hydrologic modeling, *Journal of Hydrology*, 531, 370-388. doi:10.1016/j.jhydrol.2015.08.045
- 487 Rahman, A., P. E. Weinmann, T. M. T. Hoang, and E. M. Laurenson (2002), Monte Carlo simulation of flood frequency
488 curves from rainfall, *Journal of Hydrology*, 256(3), 196-210. doi:10.1016/S0022-1694(01)00533-9
- 489 Saghafeian, B., P. Y. Julien, and F. L. Ogden (1995), Similarity in catchment response: 1. Stationary rainstorms, *Water*
490 *Resources Research*, 31(6), 1533-1541. doi:10.1029/95WR00518
- 491 Schellart, A. N. A., W. J. Shepherd, and A. J. Saul (2012), Influence of rainfall estimation error and spatial variability on
492 sewer flow prediction at a small urban scale, *Advances in Water Resources*, 45, 65-75. doi:10.1016/j.advwatres.2011.10.012
- 493 Schilling, W. (1991), Rainfall data for urban hydrology: what do we need?, *Atmospheric Research*, 27(1), 5-21.
494 doi:10.1016/0169-8095(91)90003-F
- 495 Seo, B.-C., W. F. Krajewski, A. Kruger, P. Domaszczynski, J. A. Smith, and M. Steiner (2011), Radar-rainfall estimation
496 algorithms of Hydro-NEXRAD, *Journal of Hydroinformatics*, 13(2), 277-291. doi:10.2166/hydro.2010.003
- 497 Sharif, H. O., A. A. Hassan, S. Bin-Shafique, H. Xie, and J. Zeitler (2010), Hydrologic modeling of an extreme flood in
498 the Guadalupe River in Texas, *JAWRA Journal of the American Water Resources Association*, 46(5), 881-891.
499 doi:10.1111/j.1752-1688.2010.00459.x
- 500 Sharif, H. O., S. Chintalapudi, A. A. Hassan, H. Xie, and J. Zeitler (2013), Physically Based Hydrological Modeling of the
501 2002 Floods in San Antonio, Texas, *Journal of Hydrologic Engineering*, 18(2), 228-236. doi:10.1061/(ASCE)HE.1943-
502 5584.0000475
- 503 Smith, B., J. Smith, M. Baeck, and A. Miller (2015), Exploring storage and runoff generation processes for urban flooding
504 through a physically based watershed model, *Water Resources Research*, 51(3), 1552-1569. doi:10.1002/2014WR016085
- 505 Smith, B. K., J. A. Smith, M. L. Baeck, G. Villarini, and D. B. Wright (2013), Spectrum of storm event hydrologic response
506 in urban watersheds, *Water Resources Research*, 49(5), 2649-2663. doi:10.1002/wrcr.20223
- 507 Smith, J. A., M. L. Baeck, K. L. Meierdiercks, A. J. Miller, and W. F. Krajewski (2007), Radar rainfall estimation for flash
508 flood forecasting in small urban watersheds, *Advances in Water Resources*, 30(10), 2087-2097.
509 doi:10.1016/j.advwatres.2006.09.007
- 510 Smith, J. A., M. L. Baeck, J. E. Morrison, P. Sturdevant-Rees, D. F. Turner-Gillespie, and P. D. Bates (2002), The regional
511 hydrology of extreme floods in an urbanizing drainage basin, *Journal of Hydrometeorology*, 3(3), 267-282.
512 doi:10.1175/1525-7541(2002)003<0267:TRHOEF>2.0.CO;2



- 513 Smith, J. A., A. J. Miller, M. L. Baeck, P. A. Nelson, G. T. Fisher, and K. L. Meierdiercks (2005a), Extraordinary Flood
514 Response of a Small Urban Watershed to Short-Duration Convective Rainfall, *Journal of Hydrometeorology*, 6(5), 599-
515 617. doi:10.1175/JHM426.1
- 516 Smith, J. A., M. L. Baeck, K. L. Meierdiercks, P. A. Nelson, A. J. Miller, and E. J. Holland (2005b), Field studies of the
517 storm event hydrologic response in an urbanizing watershed, *Water Resources Research*, 41(10), W10413(10415).
518 doi:10.1029/2004wr003712
- 519 Smith, J. A., M. L. Baeck, G. Villarini, C. Welty, A. J. Miller, and W. F. Krajewski (2012), Analyses of a long-term, high-
520 resolution radar rainfall data set for the Baltimore metropolitan region, *Water Resources Research*, 48(4), 1-14.
521 doi:10.1029/2011wr010641
- 522 Wilson, C. B., J. B. Valdes, and I. Rodriguez-Iturbe (1979), On the influence of the spatial distribution of rainfall on storm
523 runoff, *Water Resources Research*, 15(2), 321-328. doi:10.1029/WR015i002p00321
- 524 Wright, D. B., J. A. Smith, and M. L. Baeck (2014a), Flood frequency analysis using radar rainfall fields and stochastic
525 storm transposition, *Water Resources Research*, 50(2), 1592-1615. doi:10.1002/2013WR014224
- 526 Wright, D. B., R. Mantilla, and C. D. Peters-Lidard (2017), A remote sensing-based tool for assessing rainfall-driven
527 hazards, *Environmental Modelling & Software*, 90, 34-54. doi:10.1016/j.envsoft.2016.12.006
- 528 Wright, D. B., G. Yu, and J. F. England (2020), Six decades of rainfall and flood frequency analysis using stochastic storm
529 transposition: Review, progress, and prospects, *Journal of Hydrology*, 585, 124816. doi:10.1016/j.jhydrol.2020.124816
- 530 Wright, D. B., J. A. Smith, G. Villarini, and M. L. Baeck (2013), Estimating the frequency of extreme rainfall using weather
531 radar and stochastic storm transposition, *Journal of Hydrology*, 488, 150-165. doi:10.1016/j.jhydrol.2013.03.003
- 532 Wright, D. B., J. A. Smith, G. Villarini, and M. L. Baeck (2014b), Long-term high-resolution radar rainfall fields for urban
533 hydrology, *Journal of the American Water Resources Association*, 50(3), 713-734. doi:10.1111/jawr.12139
- 534 Yang, L., J. A. Smith, M. L. Baeck, and Y. Zhang (2016), Flash flooding in small urban watersheds: Storm event hydrologic
535 response, *Water Resources Research*, doi:doi:10.1002/2015WR018326. doi:10.1002/2015WR018326
- 536 Younger, P. M., J. E. Freer, and K. J. Beven (2009), Detecting the effects of spatial variability of rainfall on hydrological
537 modelling within an uncertainty analysis framework, *Hydrological Processes*, 23(14), 1988-2003. doi:10.1002/hyp.7341
- 538 Yu, G., D. B. Wright, Z. Zhu, C. Smith, and K. D. Holman (2019), Process-based flood frequency analysis in an agricultural
539 watershed exhibiting nonstationary flood seasonality, *Hydrol. Earth Syst. Sci.*, 23(5), 2225-2243. doi:10.5194/hess-23-
540 2225-2019
- 541 Zhou, Z., J. A. Smith, D. B. Wright, M. L. Baeck, and S. Liu (2019), Storm catalog-based analysis of rainfall heterogeneity
542 and frequency in a complex terrain, *Water Resources Research*, 55(3), 1871-1889. doi:10.1029/2018WR023567



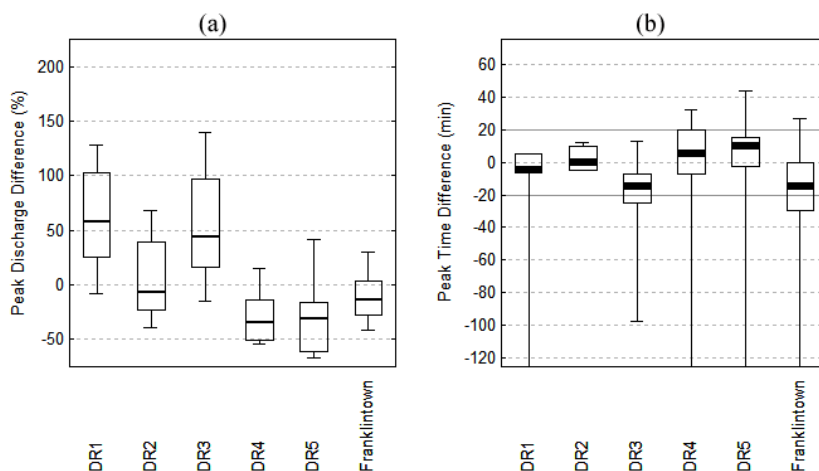
543 Zhou, Z., J. A. Smith, L. Yang, M. L. Baeck, M. Chaney, M.-C. Ten Veldhuis, H. Deng, and S. Liu (2017), The complexities
544 of urban flood response: Flood frequency analyses for the Charlotte Metropolitan Region, *Water Resources Research*, 53(8),
545 7401-7425. doi:10.1002/2016WR019997
546 Zhu, Z., D. B. Wright, and G. Yu (2018), The Impact of Rainfall Space-Time Structure in Flood Frequency Analysis, *Water*
547 *Resources Research*, 54(11), 8983-8998. doi:10.1029/2018wr023550
548 Zoccatelli, D., M. Borga, A. Viglione, G. B. Chirico, and G. Blöschl (2011), Spatial moments of catchment rainfall: rainfall
549 spatial organisation, basin morphology, and flood response, *Hydrology and Earth System Sciences*, 15(12), 3767-3783.
550 10.5194/hess-15-3767-2011
551
552



553

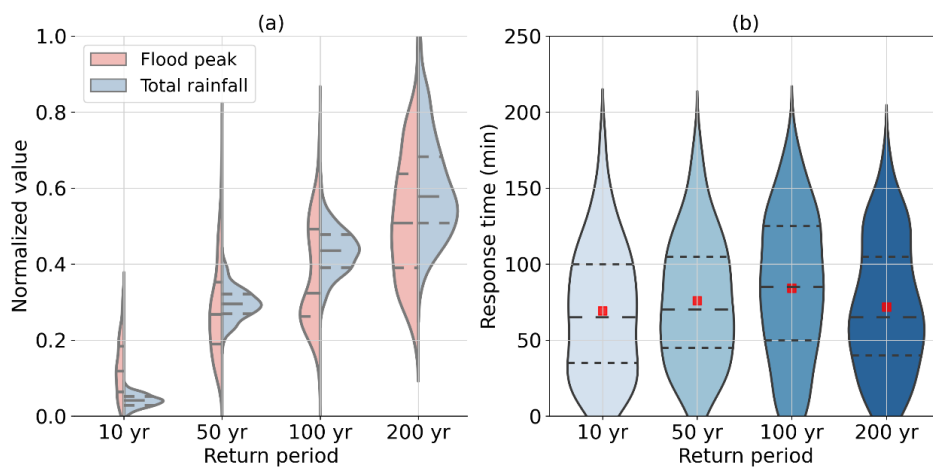


554 **Figure 1. Overview of Dead Run study region including (a) location of DR, elevation, and transposition domain of**
555 **SST; (b) land use land cover and stream gages. Land use land cover was obtained from the National Land Cover**
556 **Data set (NLCD, <http://www.mrlc.gov>)**



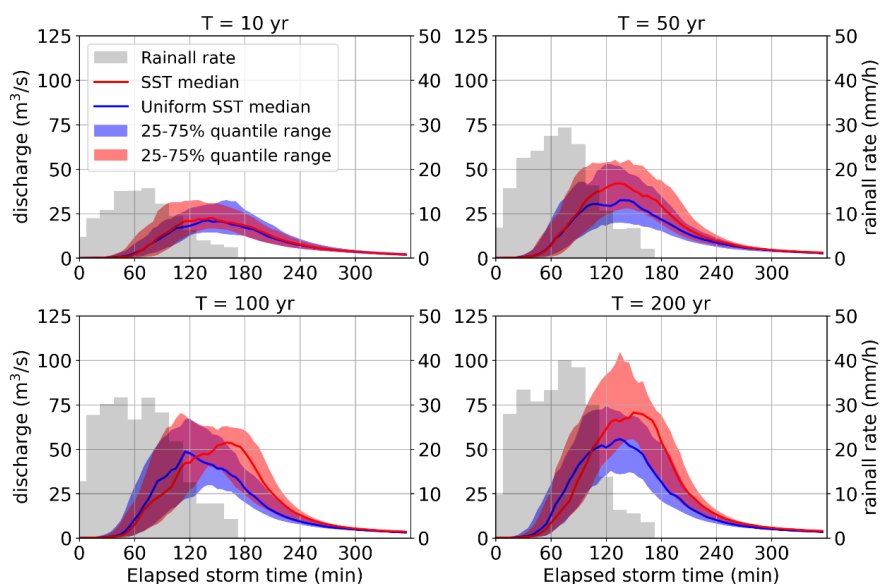
557

558 **Figure 2. Comparison of (a) flood peak discharges and (b) response times for 21 historical rainfall events.**

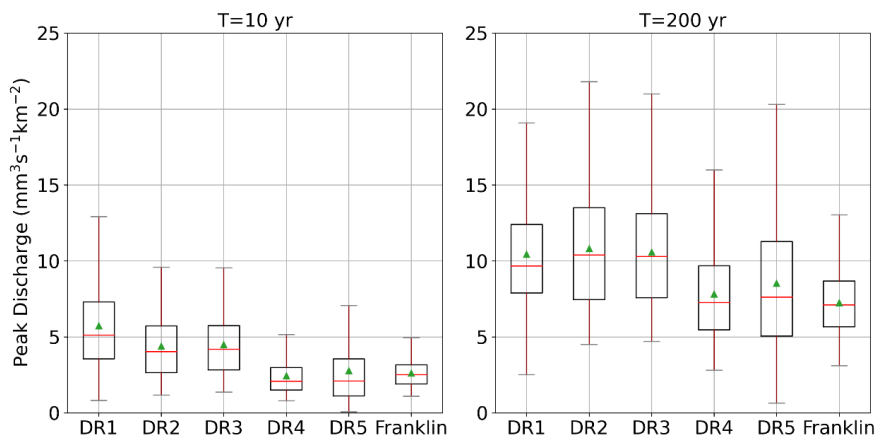


559

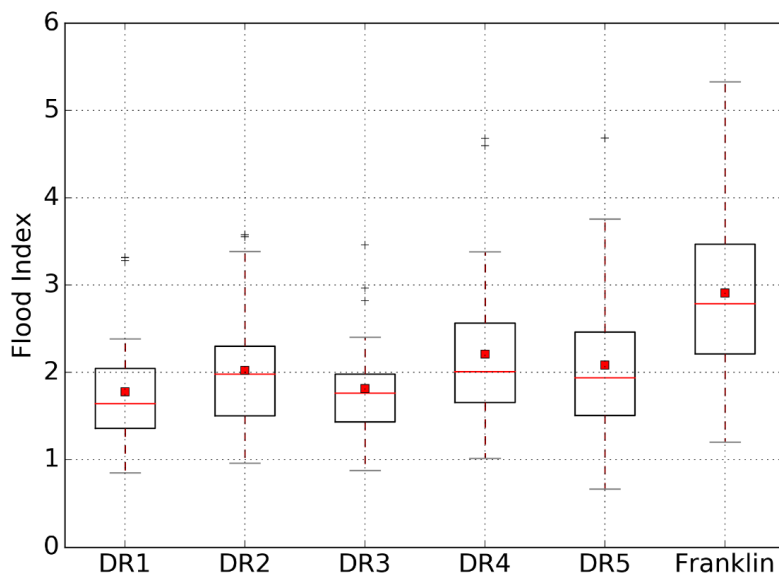
560 **Figure 3. Violin plots of (a) normalized flood peak and normalized total rainfall; and (b) response time based on the**
561 **3-h design storms from 10-y to 200-y return periods. (The red dot indicates mean value. Dashed line in the middle**
562 **indicates the median value. Upper and lower dashed lines indicate the 75th and 25th quantiles, respectively.)**



563
 564 **Figure 4.** Time series of simulated hydrographs for Franklintown based on the 3-h design storms from 10-yr to 200-
 565 yr return periods with spatially uniform (blue) and spatially distributed (red) rainfall. The grey bar indicates the
 566 median value of basin-averaged rainfall rate.

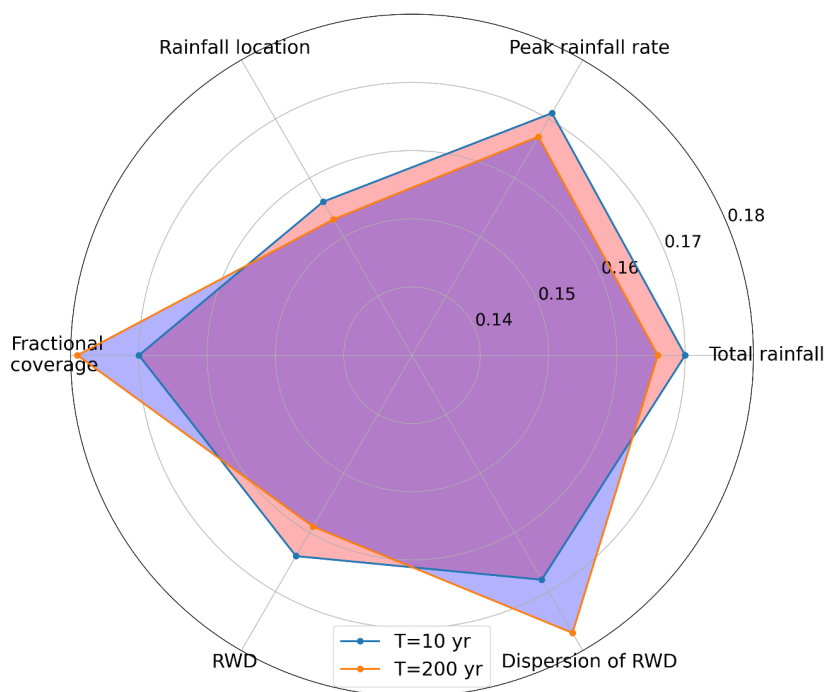


567
 568 **Figure 5.** Boxplots of normalized flood peaks for Franklintown and five subwatersheds.



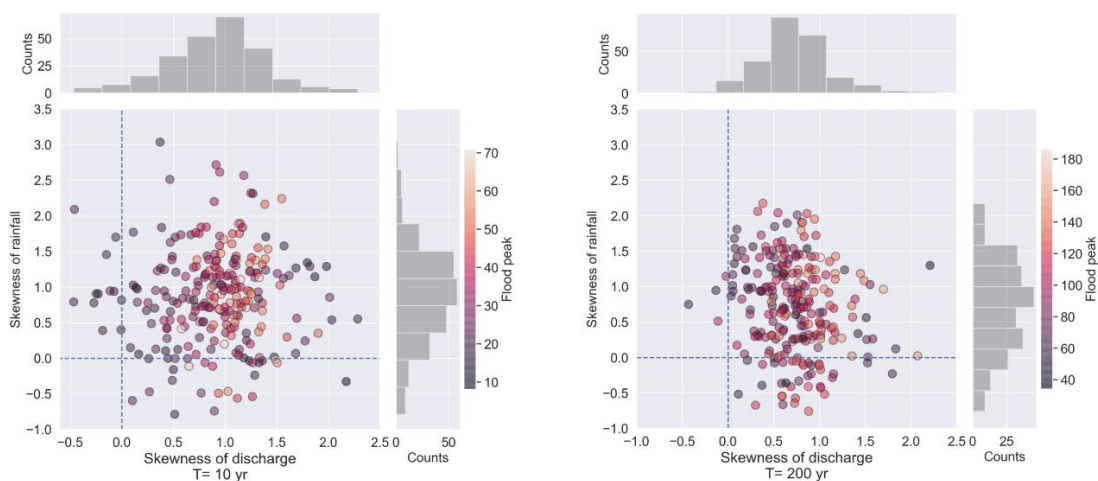
569
 570

Figure 6. Boxplot of flood index across the DR subwatersheds for the 100-yr design storms.



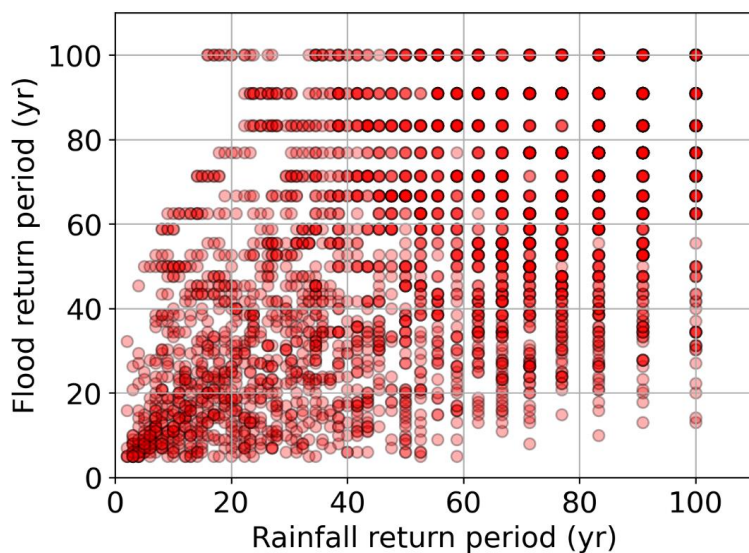
571
 572
 573

Figure 7. Feature importance analysis of RF model for space-time rainfall structure and 10-yr (red) and 200-yr (blue) flood peaks.



574

575 **Figure 8. Scatter plots of skewness of rainfall and peak discharge—left: 10-yr return period; right: 200-yr return**
 576 **period.**



577

578 **Figure 9. Scatterplot comparison return periods for rainfall and peak discharge for individual SST-based**
 579 **simulations.**

580

581 **Table 1: Characteristics of Dead Run watershed.**

	USGS ID	Area (km ²)	Developed Land (%)	Imperviousness (%)	Controlled area (%)



DR1	01589317	1.32	99%	73.6	41.9
DR2	01589316	1.92	98%	55.5	18.5
DR3	01589320	4.95	98%	62.2	24.4
DR4	01589315	6.29	98%	51.5	12.2
DR5	01589312	2.05	96%	47.9	3.2
Franklinton	01589330	14.3	96%	52.3	25.1

582 **Table 2. The median flood peak reductions using spatially uniform and spatially distributed**
 583 **rainfall.**

	T=10 yr	T=50 yr	T=100 yr	T=200 yr
DR1	14%	20%	13%	26%
DR2	19%	40%	28%	42%
DR3	24%	33%	27%	31%
DR4	32%	51%	38%	35%
DR5	15%	75%	37%	30%
Franklin	22%	36%	31%	42%

584